Electronic Supporting Information (ESI)

Functionalized Metal-Organic Framework Modified Membrane with Ultralong Cyclability and Superior Capacity for Zinc/Bromine Flowless Battery

Dabin Han[a], Kyungjae Shin[b], Hee-Tak Kim[b] and Sangaraju Shanmugam[a*]

[a]Department of Energy Science & Engineering, Daegu Gyeongbuk Institute of Science & Technology (DGIST), Daegu 42988, Republic of Korea.
[b]Department of Chemical and Biomolecular Engineering, Korea Advanced Institute of Science and Technology (KAIST), Daejeon 34141, Republic of Korea.

*E-mail: sangarajus@dgist.ac.kr

Table of Contents

Table S1. Summary of performance comparison previously reported and this work in the ZBFLB.

Modification	Current density (mA cm^{-2})	Charged capacity (mAh cm^{-2})	CE (%)	EE (%)	Cycle number	Cycle life (h)	Ref.
Viologen modified electrode	10	24.3	96	85	400	1905	[1]
N doped porous carbon electrode	5	5	85.0	80.0	1000	1000	[2]
Exfoliated COF	6.7	0.73	99	-	218	1000	[3]
Br_2 complex additive with porous electrode	15	1	99.9	94.0	11,000	733	[4]
High concentration of $ZnBr_2$ electrolyte	5	1	95.0	79.0	2500	1666	[5]
Polybromide confiner-modified electrode	8	2	92.1	74.5	1200	1000	[6]
CCl_4 additive in electrolyte	5	0.8	96.0	81.0	200	67	[7]
Functionalized MOF composite membrane	10	2.46	98.0	81.0	5000	2460	This work
	10	24.6	93.2	80.7	20	95	
	10	98.45	78.7	69.1	70	1200	

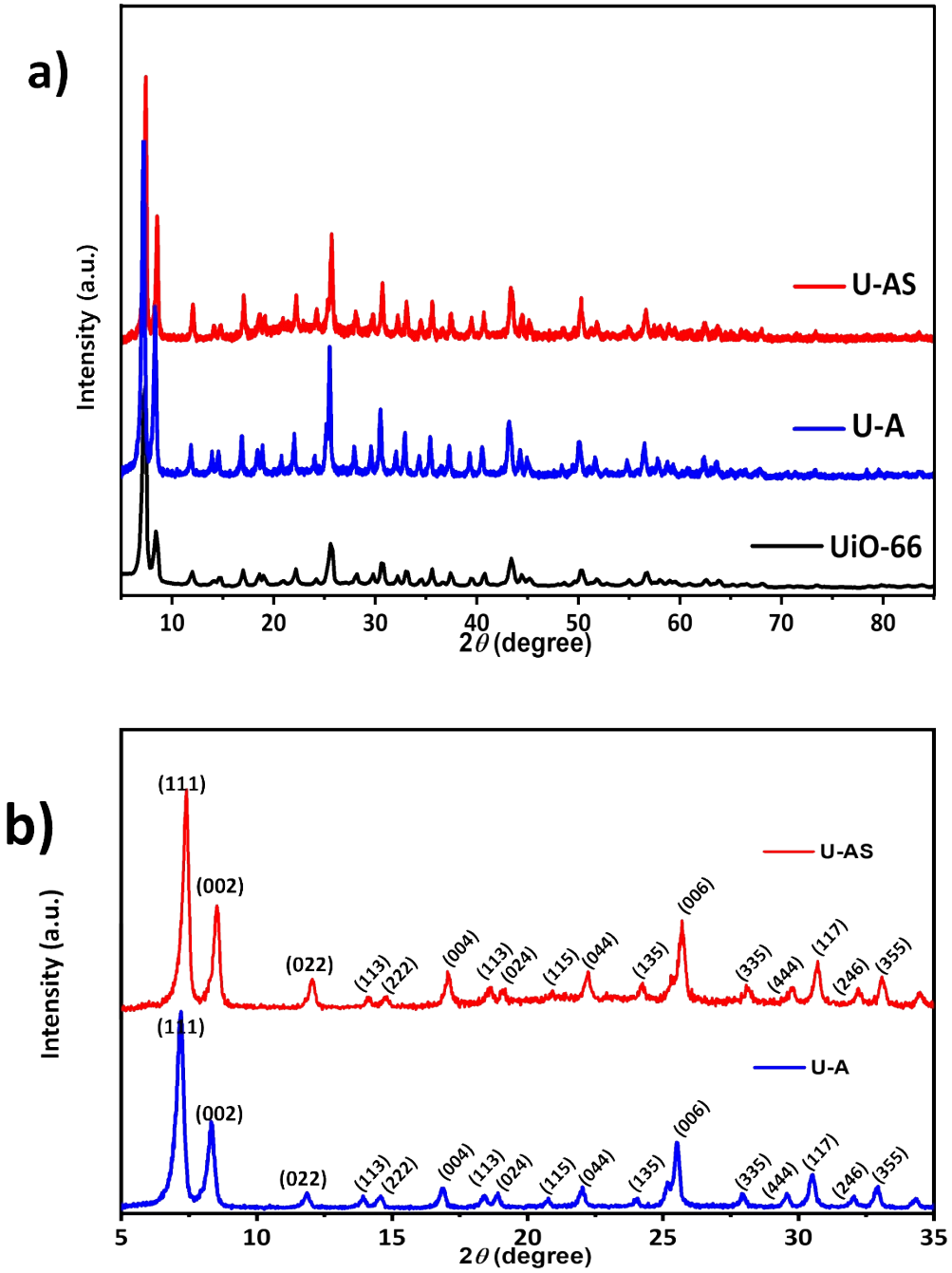

Fig. S1 The XRD results of (a) UiO-66, U-A and U-AS, and (b) Miller indices of U-A and U-AS.

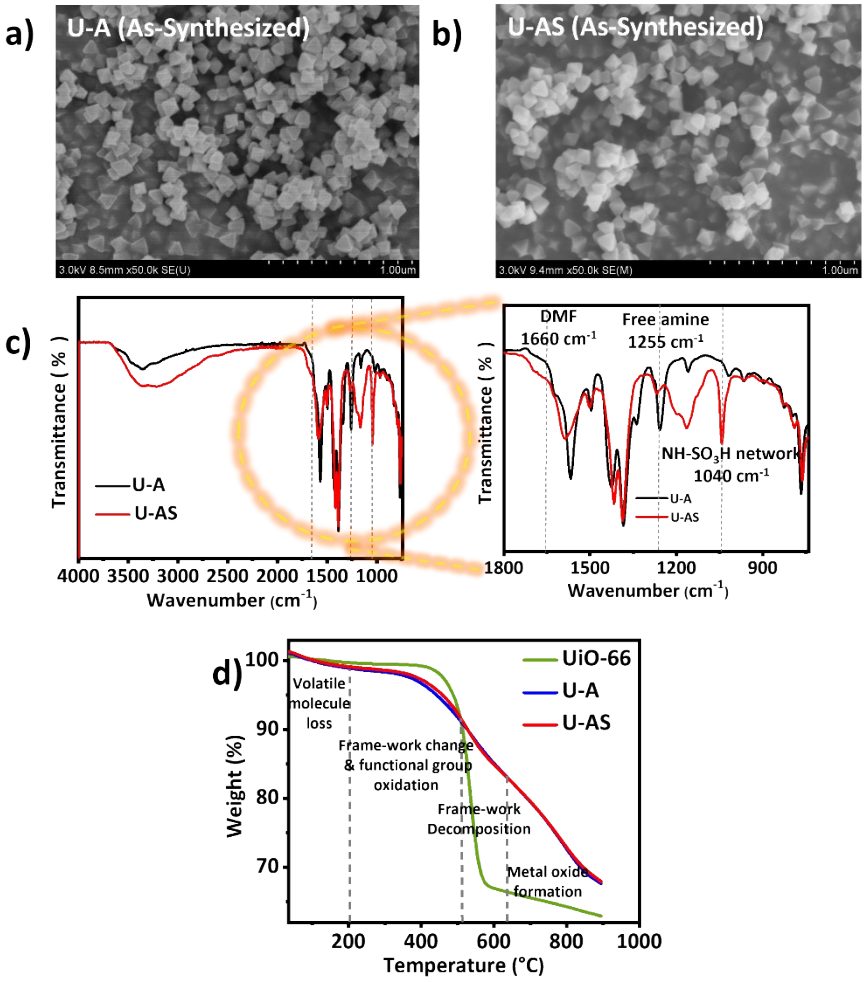

Fig. S2 SEM images of (a) U-A as-synthesized and (b) U-AS as-synthesized. (c) FT-IR results of U-A and U-AS. (d) TGA curves of UiO-66, U-A and U-AS.

Due to the functional groups, U-A and U-AS showed significantly different thermal decomposition behavior from UiO-66 in Fig. S2d. In addition, U-A and U-AS showed a similar trend in TGA results. The adsorbed volatile molecules were evaporated up to about 200 °C. The U-A and U-AS showed more weight loss than the UiO-66 in this region, with more guest water molecules in the pores or OH groups due to the $-NH_2$ and $-SO_3H$ functional groups. In particular, the U-AS sample showed a slower weight drop than the U-A from 200 to 500 °C. This may be due to the oxidation of the pendant alkyl and $-SO_3H$ groups in the U-AS. As the 2-aminoterephthalic acid or terephthalic acid was decomposed, the framework structure was disintegrated between 500 and 650 °C. U-A and U-AS showed less weight

loss than UiO-66. The framework of UiO-66 was completely decomposed before 600 °C, whereas the framework of U-A and U-AS was maintained even after 600 °C due to the presence of -NH_2 group, which is more stable in an N_2 condition.

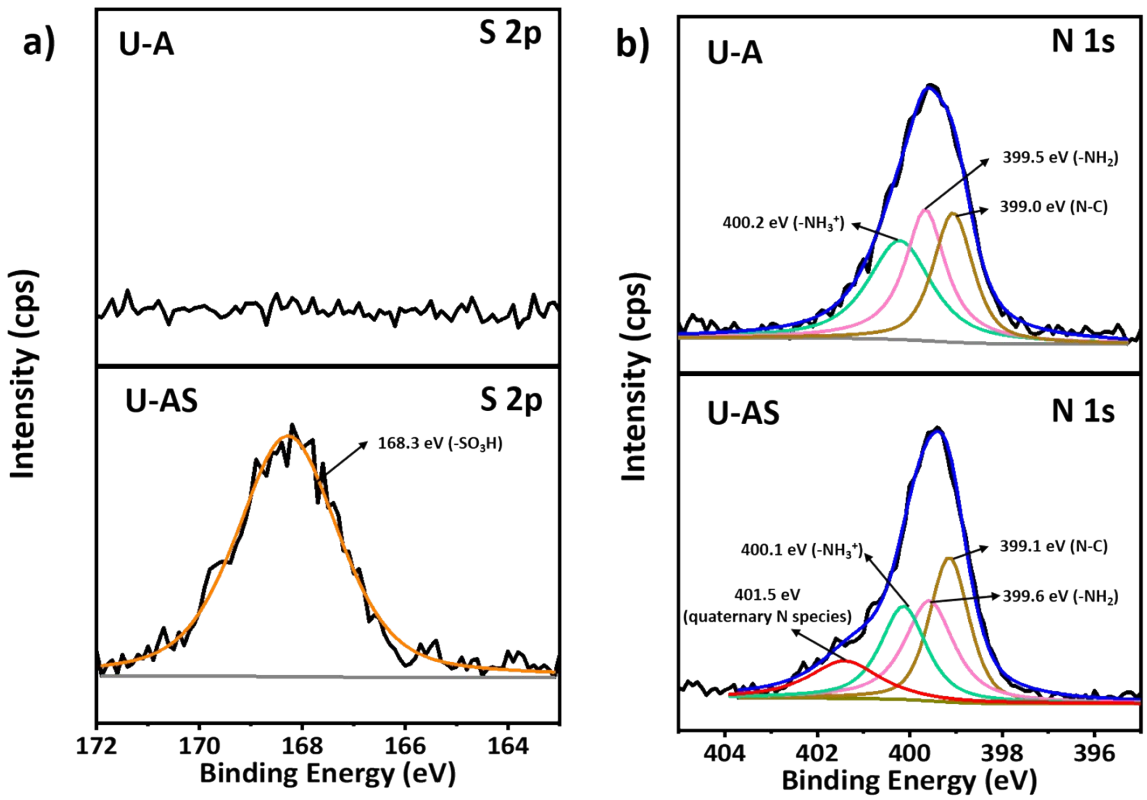

Fig. S3 High-resolution (a) S2p spectrum of U-A and U-AS; (b) N1s spectrum of U-A and U-AS in XPS.

Table S2. The CHNS elemental analysis of UiO-66, U-A and U-AS.

	C (%)	H (%)	N (%)	S (%)
UiO-66	35.81	2.21	-	-
U-A	32.74	2.93	5.02	-
U-AS	39.50	4.05	4.06	10.44

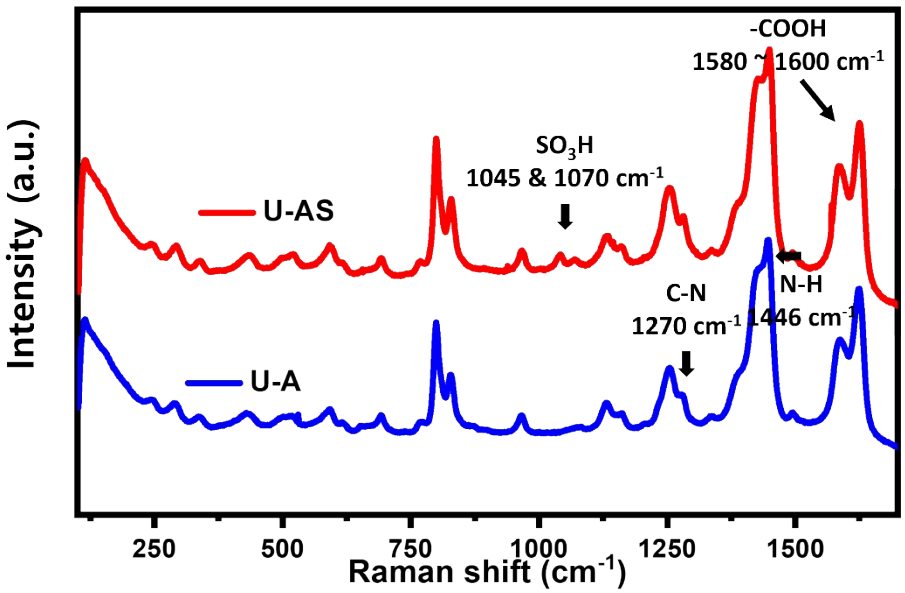

Fig. S4 Raman spectrum of U-A and U-AS as-synthesized.

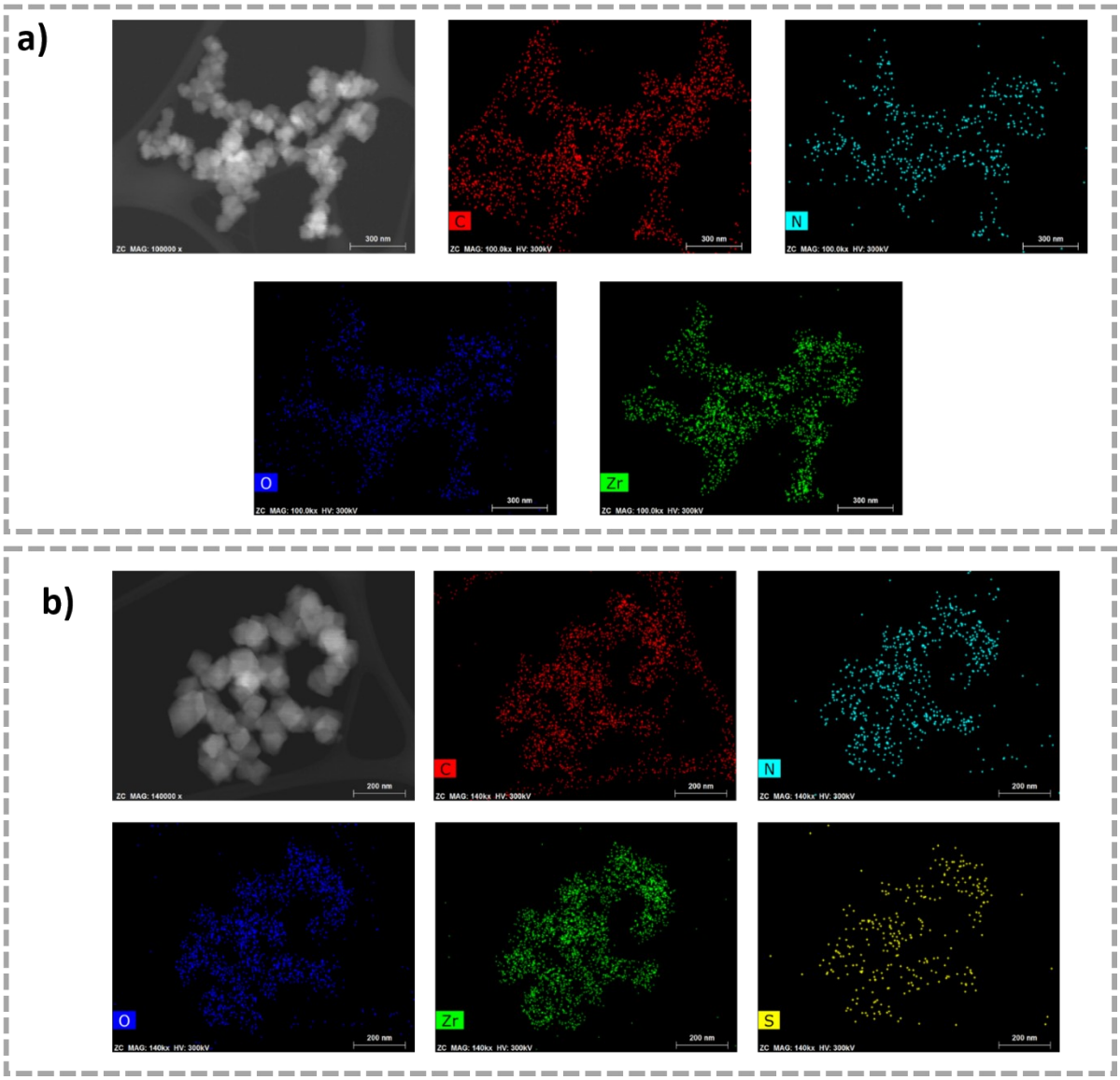

Fig. S5 TEM image and element mapping images of (a) U-A for C, N, O, Zr and (b) U-AS for C, N, O, Zr, S.

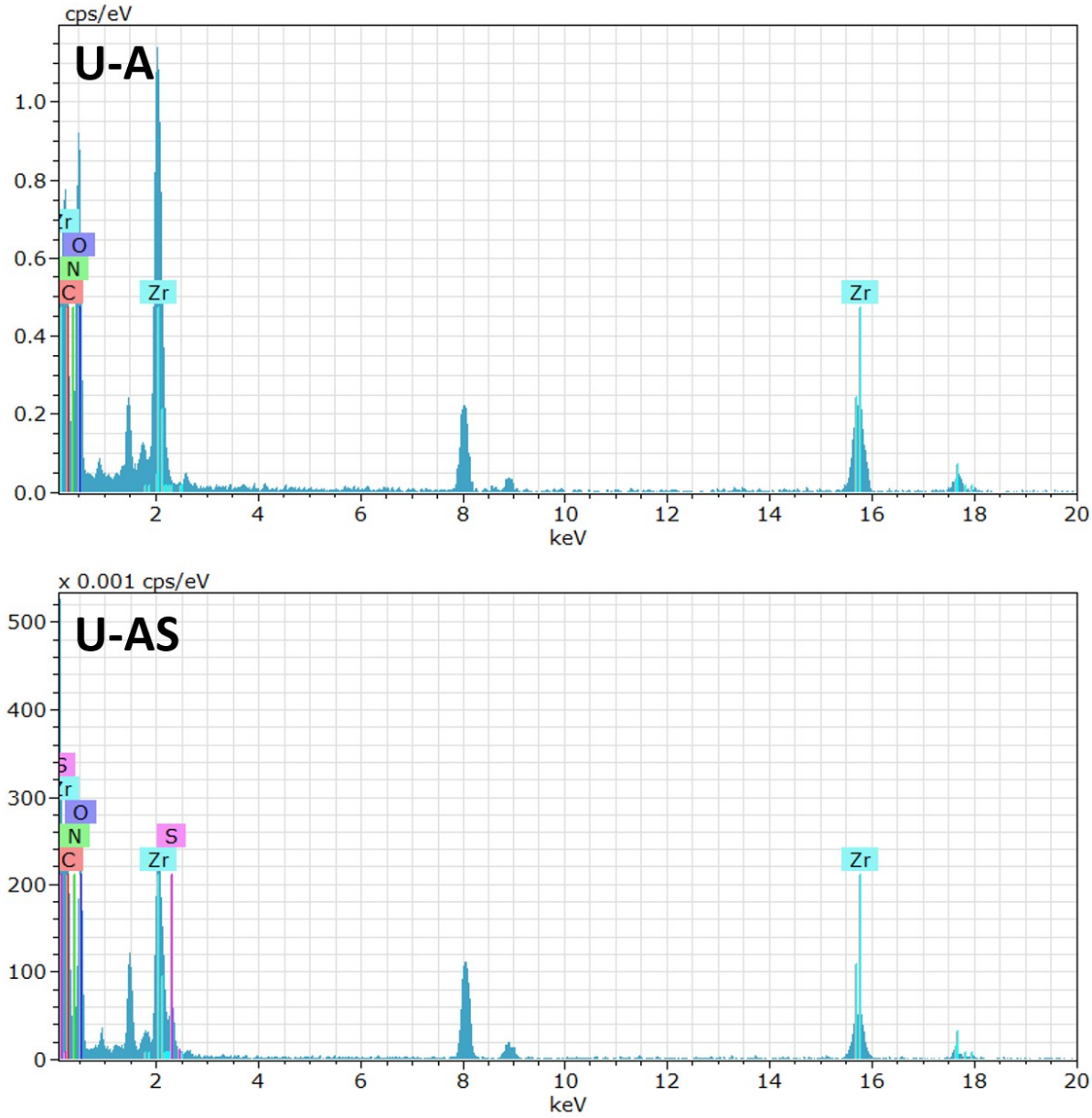

Fig. S6 EDX spectrum of U-A and U-AS.

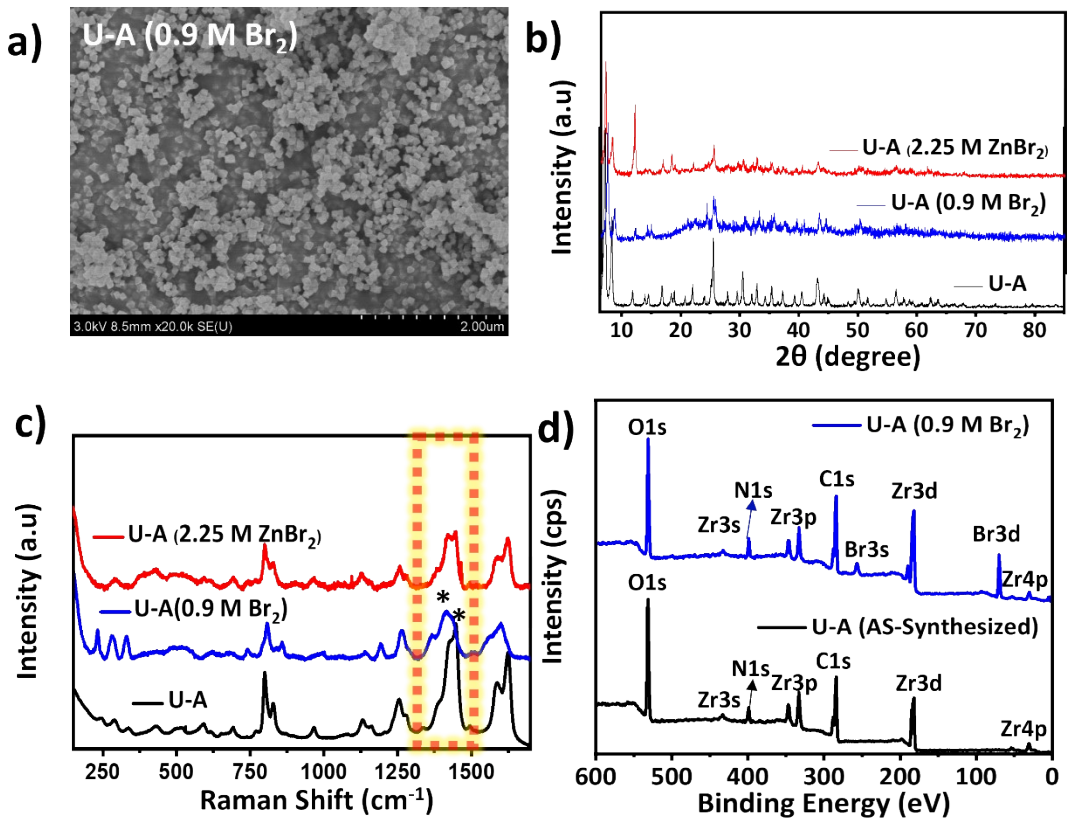

Fig. S7 After hydrolytic stability test of U-A; (a) SEM images of U-A under 0.9 M Br_2 solution, (b) XRD patterns of U-A, (c) Raman spectrum of U-A and (d) XPS spectrum of U-A.

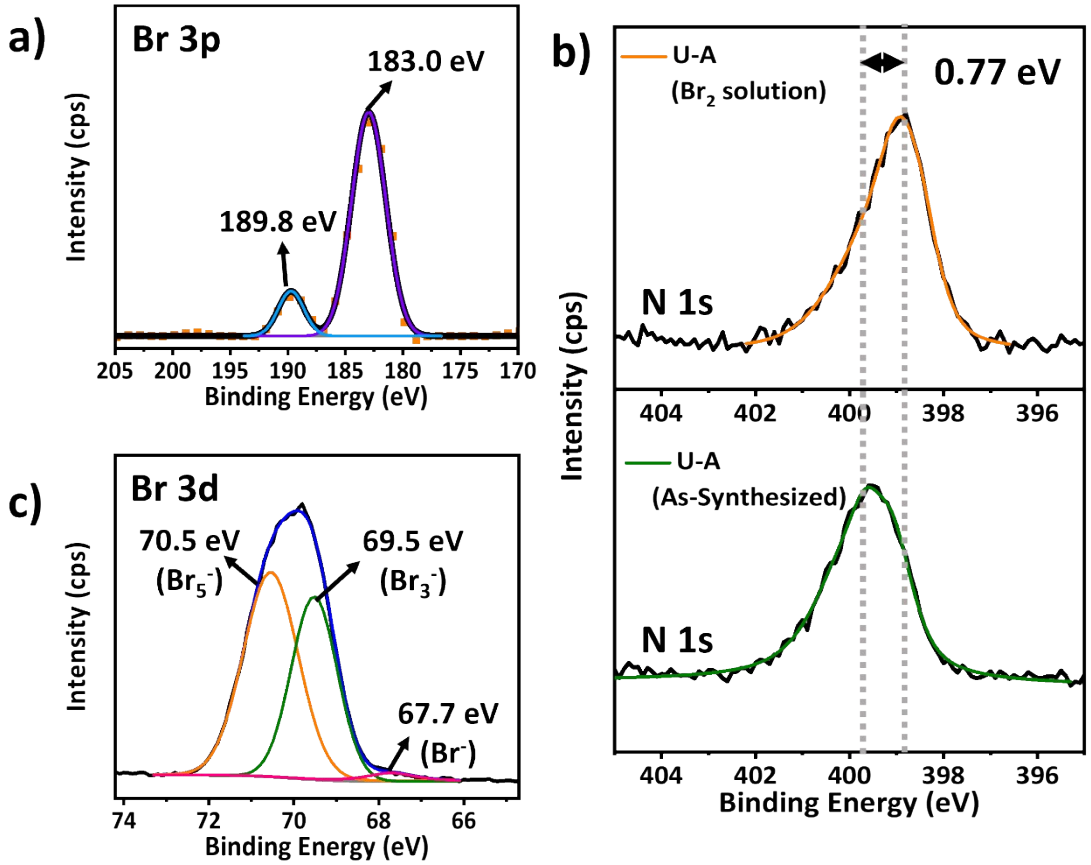

Fig. S8 XPS spectrum after hydrolytic stability test of U-A in 0.9 M Br_2 solution; (a) fitted Br 3p, (b) fitted N1s and (c) fitted Br 3d.

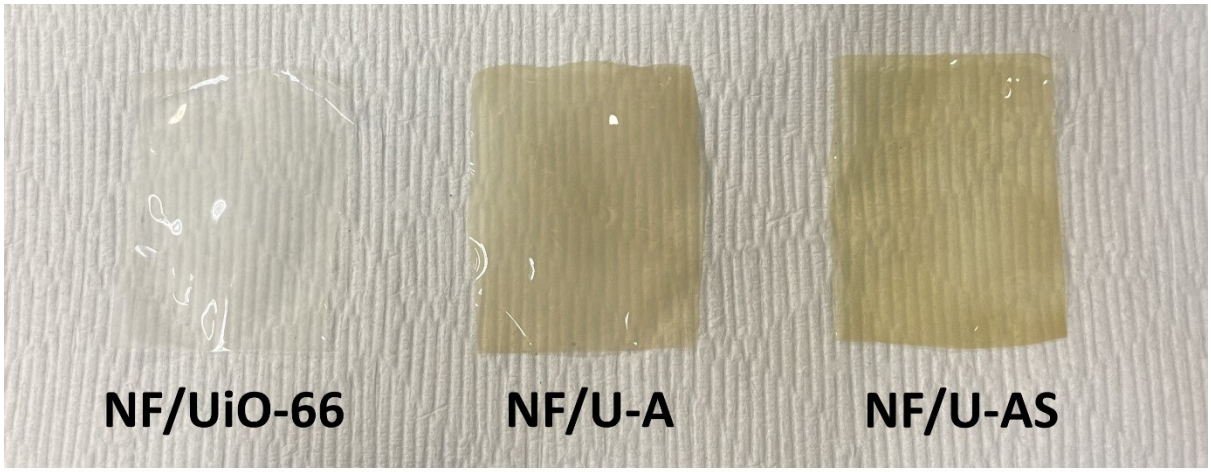

Fig. S9 Images of NF/UiO-66, NF/U-A and NF/U-AS membranes.

Table S3. Properties of membranes.

Membranes	Water uptake (%)	Contact angle (°)	Ion transport number (t_+)	Hydrophilic domain size (nm)	Ion conductivity (mS cm^{-1})	Br_2 concentration at 12 h (mM L^{-1})
NRE-212	24.20	58.55	0.30	4.43	12.37	59.67
NF/UiO-66	23.15	68.62	0.37	4.60	5.12	51.59
NF/U-A	21.86	67.67	0.67	4.08	3.38	35.79
NF/U-AS	34.12	31.21	0.51	3.91	12.21	44.05

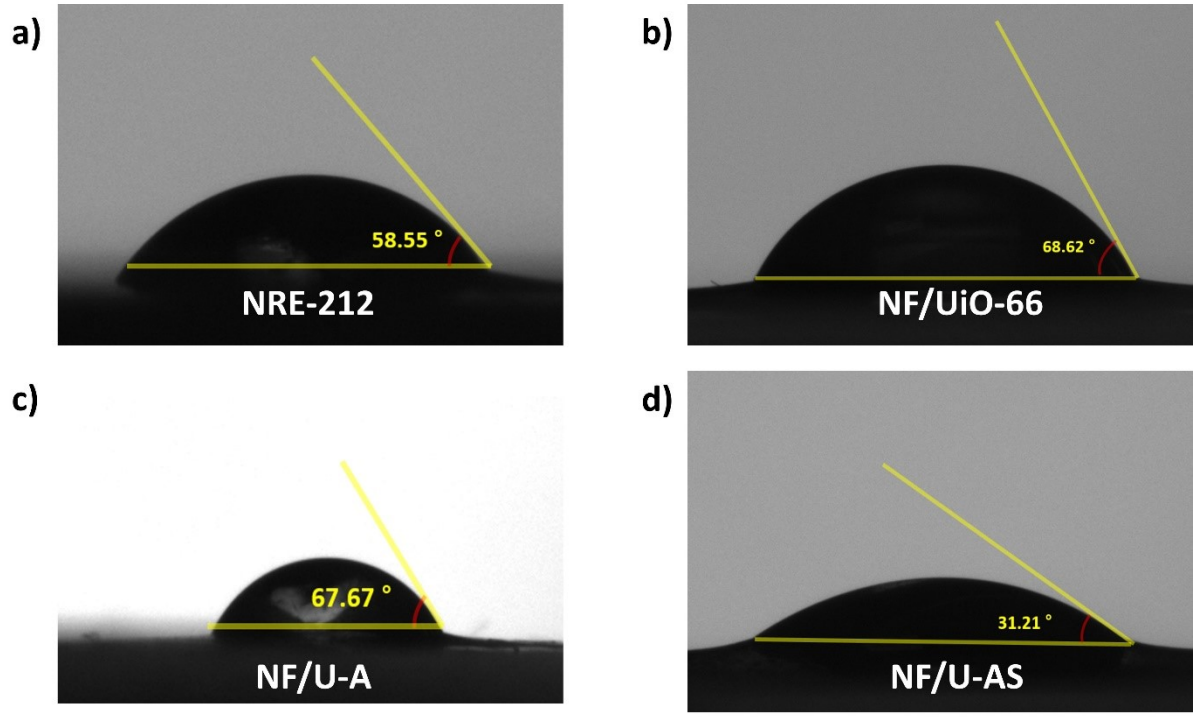

Fig. S10 Contact angle of membranes; (a) NRE-212, (b) NF/UiO-66, (c) NF/U-A and (d) NF/U-AS.

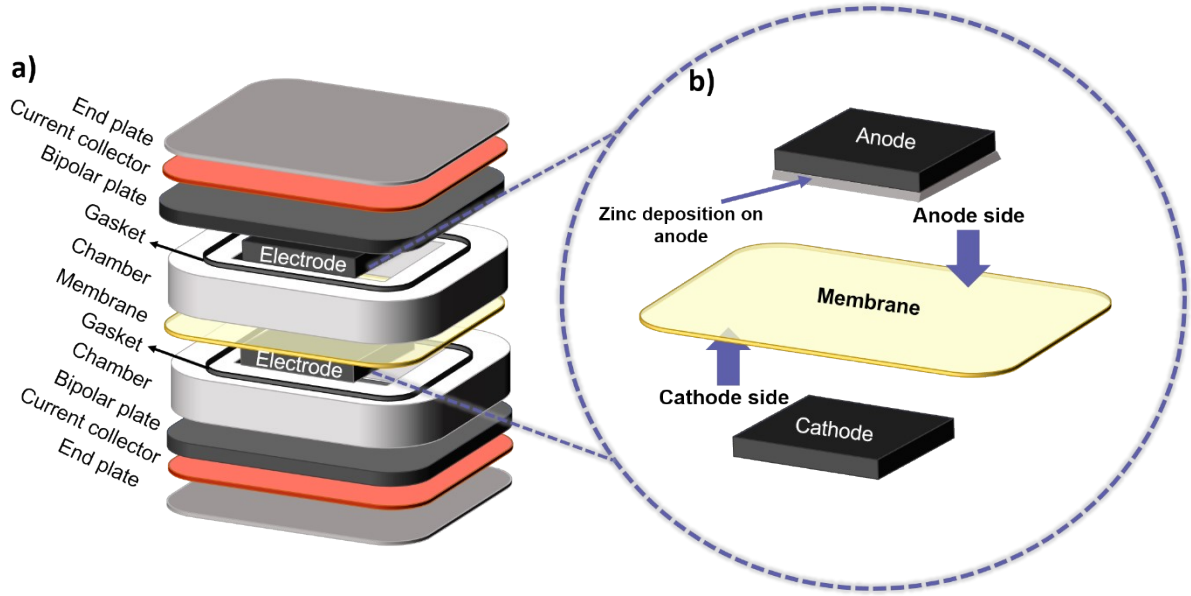

Fig. S11 Schematic of (a) Zinc/Bromine flowless single cell and (b) membrane sandwiched between anode and cathode.

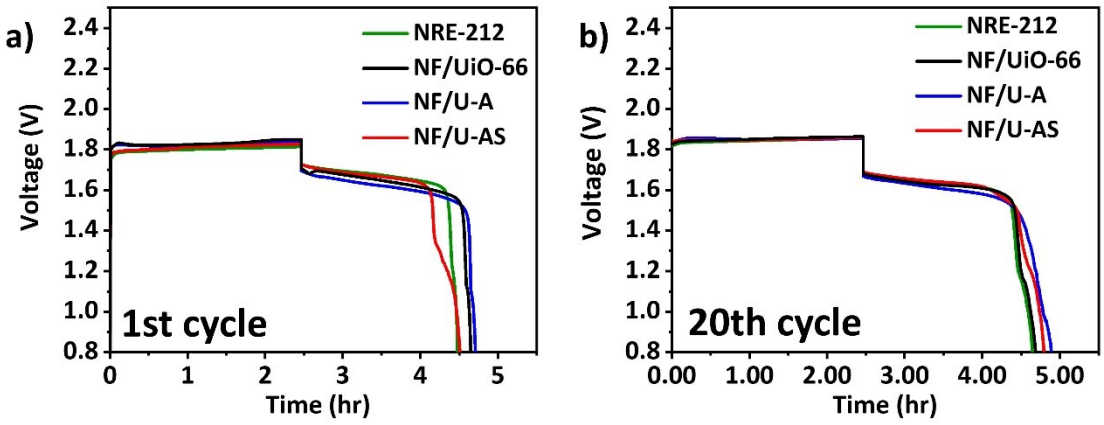

Fig. S12 Charge-discharge voltage curves of ZBFLB at 10% DOC (a) 1st cycle and (b) 20th cycle.

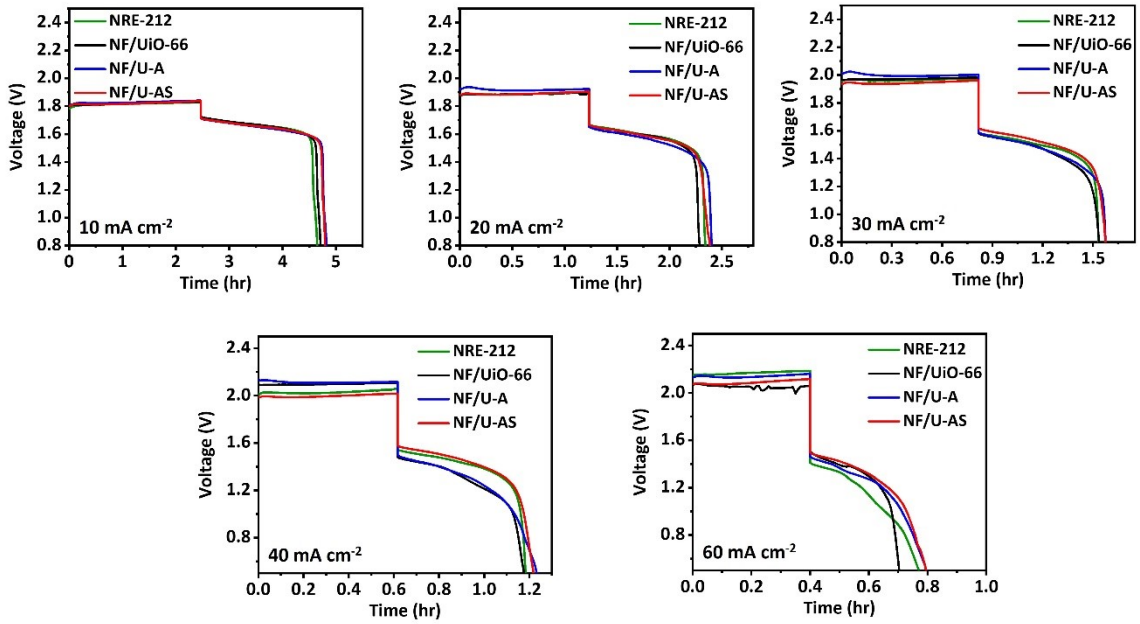

Fig. S13 Charge-discharge voltage curves of ZBFLB depending on current density at 10% DOC.

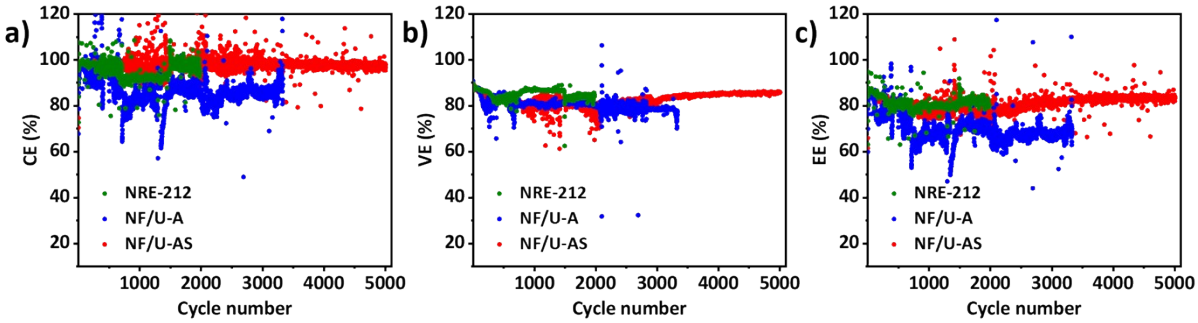

Fig. S14 The ZBFLB performance test with 1% DOC at 10 mA cm^{-2}: (a) CE, (b) VE and (c) EE.

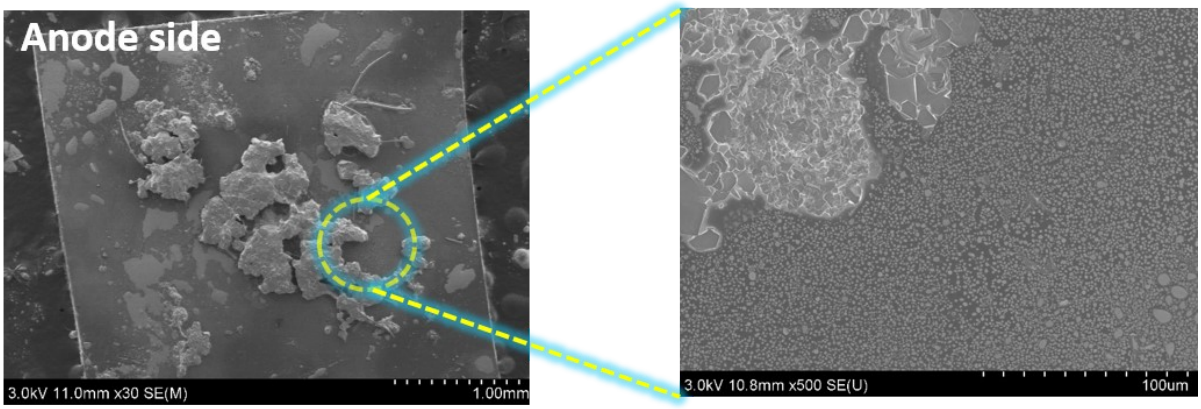

Fig. S15 FE-SEM images of NF/U-A surface after about 3000 cycles at 1% DOC with 10 mA cm^{-2}.

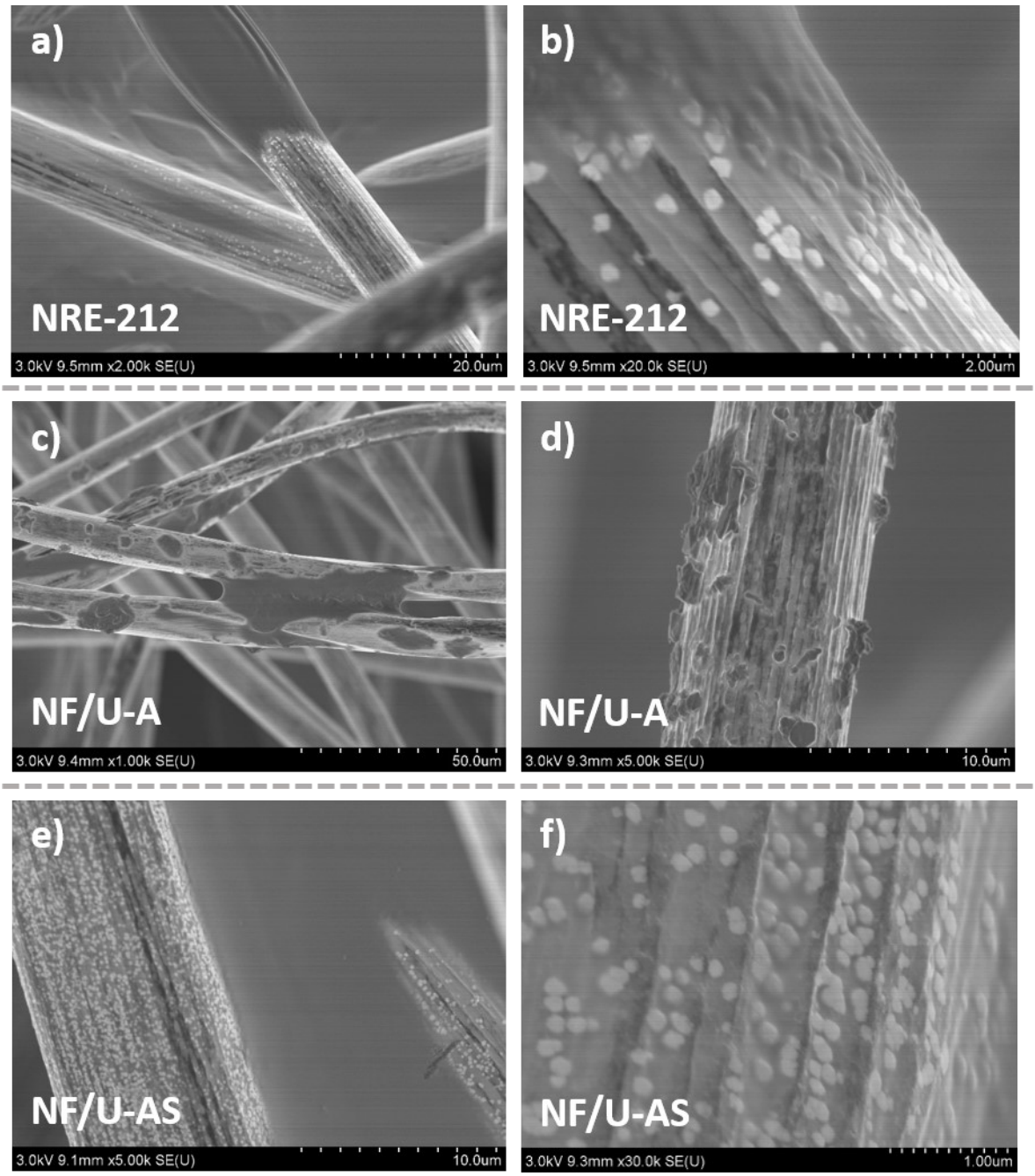

Fig. S16 FE-SEM images of Zn deposition on anode at 1% DOC. (a, b) NRE-212, (c, d) NF/U-AS and (e, f) NF/U-AS were applied to ZBFLB, respectively.

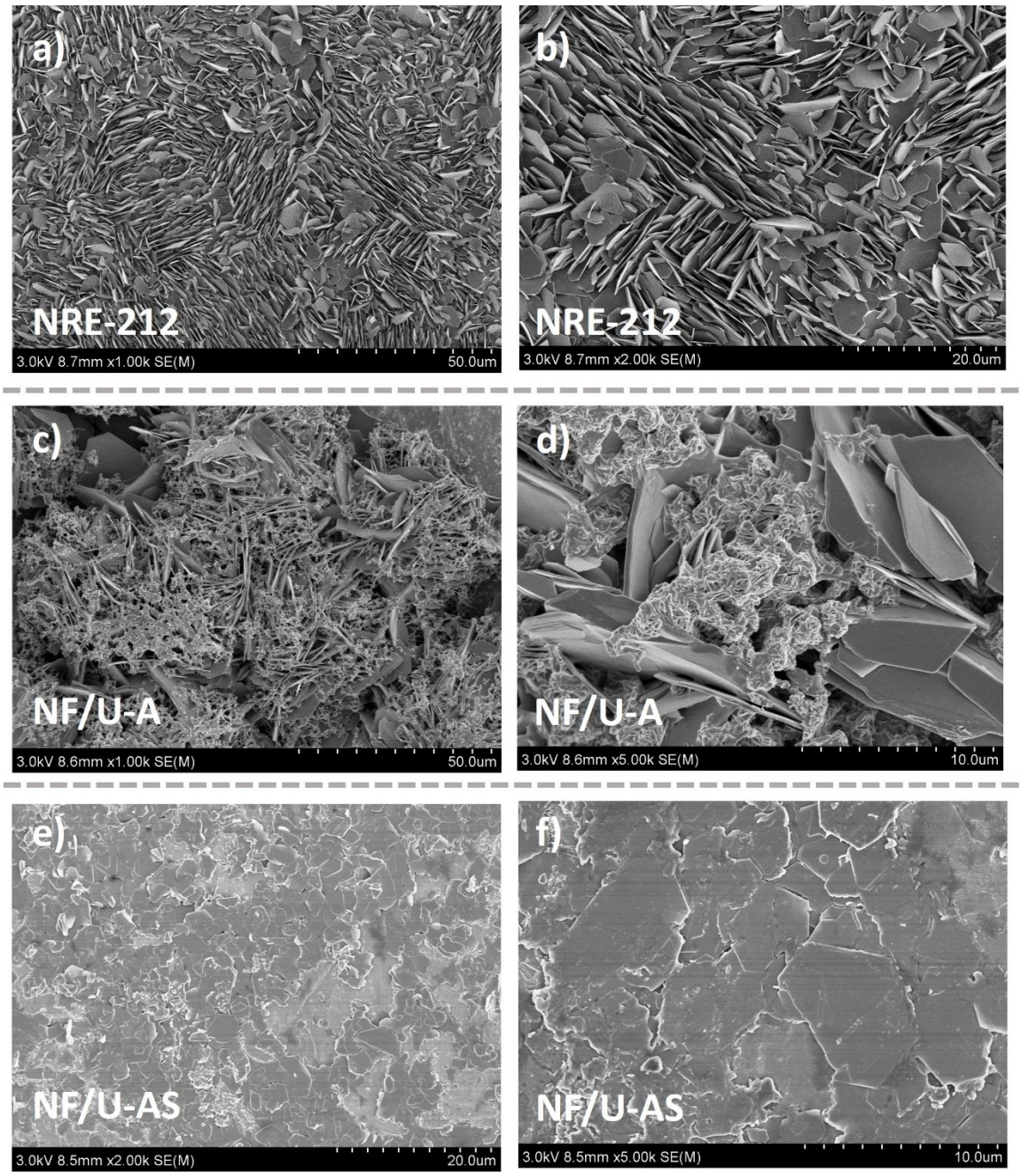

Fig. S17 FE-SEM images of Zn deposition in Zn symmetric cells at 1 mAh cm^{-2} with 1 mA cm^{-2} after 5 cycles: (a, b) NRE-212, (c, d) NF/U-AS and (e, f) NF/U-AS.

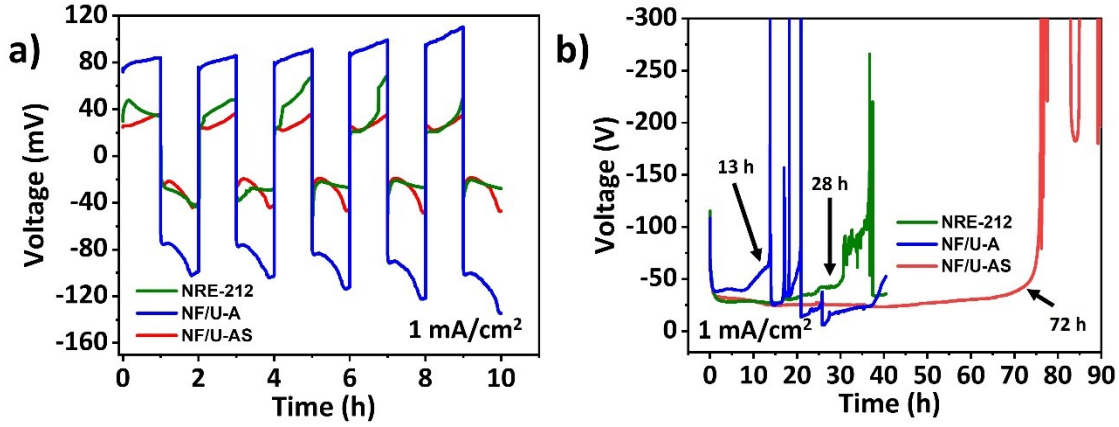

Fig. S18 (a) Cycling of Zn symmetric cell employing NRE-212, NF/U-A, and NF/U-AS, (b) Chronopotentiometry of Zn symmetric cells at 1 mA cm^{-2} for short-circuit time measurement depending on membranes.

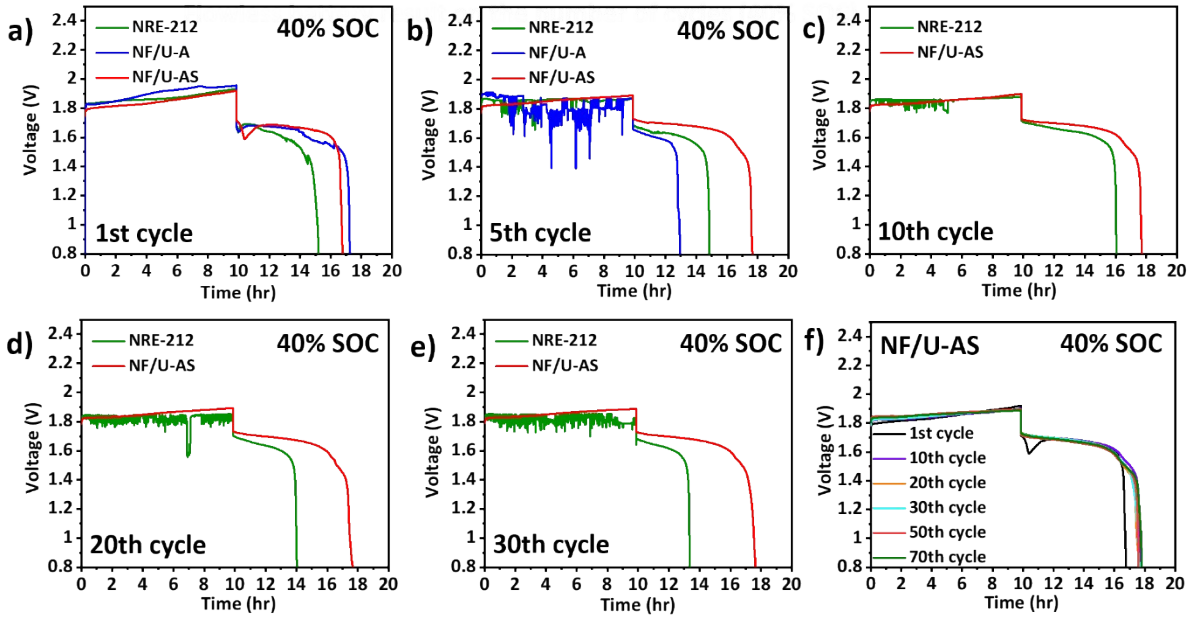

Fig. S19 Charge-discharge voltage curves of ZBFLB at 40% DOC (a) 1st cycle, (b) 5th cycle, (c) 10th cycle, (d) 20th cycle, (e) 30th cycle and (f) NF/U-AS result according to cycles.

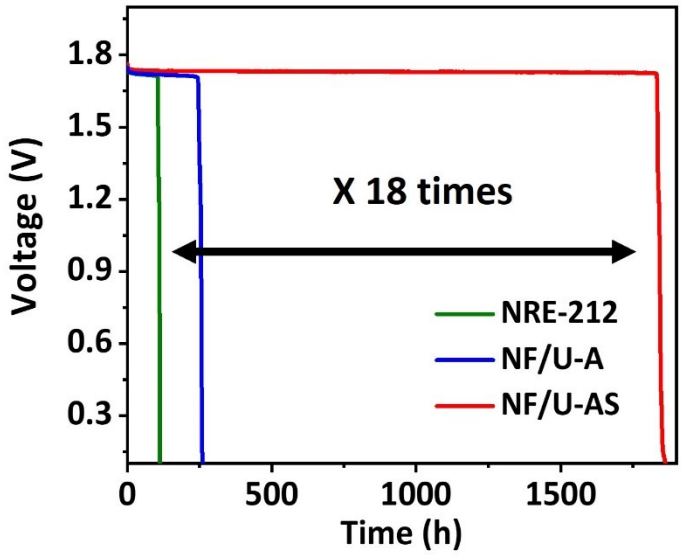

Fig. S20 The OCV decay curves of NRE-212, NF/U-A, and NF/U-AS after 40% DOC at 10 mA cm^{-2}.

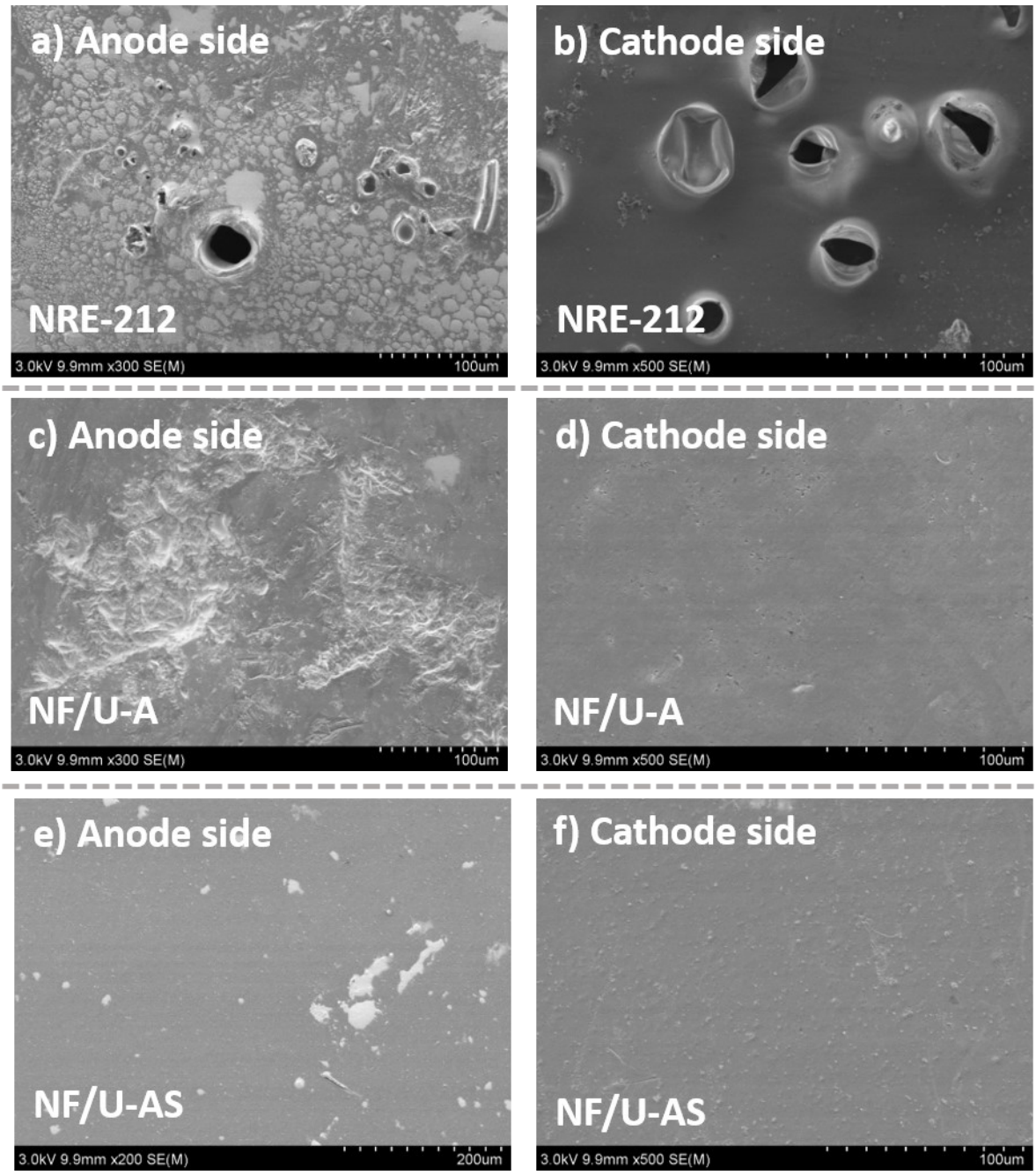

Fig. S21 FE-SEM images of (a, b) NRE-212, (c, d) NF/U-A and (e, f) NF/U-AS surfaces after cyclability test at 40% DOC.

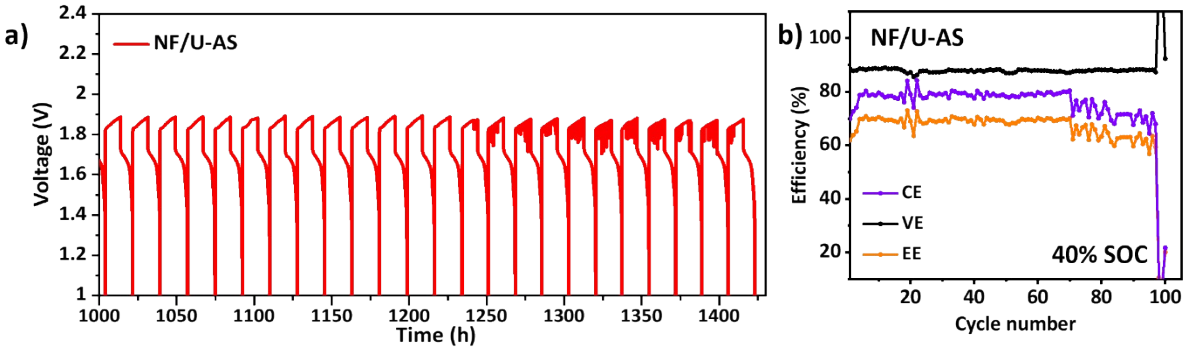

Fig. S22 The cyclability results of NF/U-AS at 40% DOC with 10 mA cm^{-2} of (a) charge-discharge profile and (b) CE, VE, EE results.

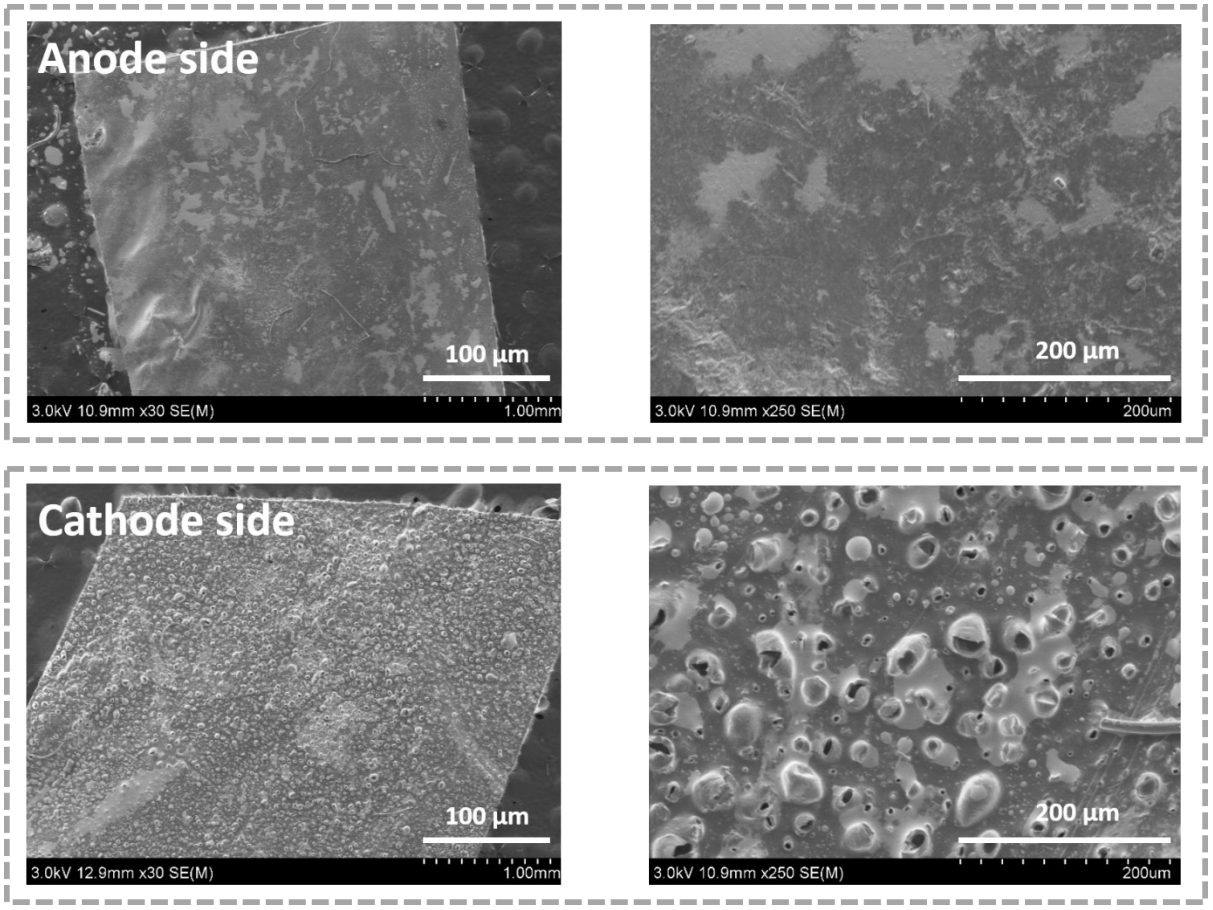

Fig. S23 FE-SEM images of NF/U-AS after cyclability test at 40% DOC over 1400 h.

Experiment

The ion conductivity (δ) of membranes was obtained by dividing the area resistance of the membrane thickness from the area resistance values. The area resistance was measured without carbon-felt electrodes in the flowless single cell. The membrane is divided into two compartments with an effective area of 3.92 cm^2. The two compartments were filled out fully with 2.25 $ZnBr_2$ + 0.5 M $ZnCl_2$. The area resistance was evaluated with an electrochemical impedance analyzer (biologic potentiostat analyzer) at an amplitude of 10 mV in the frequency range of 1 Hz to 100 kHz. The area resistance was calculated by the formula below:

$$ASR = A \times (r_1 - r_2)$$

Where A is the effective area, r_1 is the ohmic resistance of the cell with the membrane, and r_2 is solution resistance without the membrane.

Ion transport numbers of membranes were measured by the liquid junction potential of the H-type with two Ag/AgCl reference electrodes filled with a 3 M NaCl. The left and right of the cell were filled with 0.01 M $ZnBr_2$ and 0.6 M $ZnBr_2$, respectively. The Ag/AgCl electrodes were located in each cell. Using the measured open-circuit voltage (OCV) values derived from the difference in concentration of 0.01 M $ZnBr_2$ and 0.6 $ZnBr_2$ electrolytes, the transference number was obtained by the following the Eq. (1) and (2)

$$E_j = \emptyset^{\beta} - \emptyset^{\alpha} = -\frac{RT}{F}\sum_i \int_{\alpha}^{\beta} \frac{t_i}{Z_i} dlna_i, \quad (1)$$

$$t_+ + t_- = 1, \quad (2)$$

where, E_j means the liquid junction potential corresponding to OCV. R is the ideal gas constant.

T is the temperature. F is the Faraday constant. t_i is the ion transference number and z_i is the charge of the ion, a_i is the ion activity. α and β are 0.01 M and 0.6 M $ZnBr_2$, respectively.

To investigate the Zn plating behavior according to membranes, Zn symmetric cell was assembled in a 2032 coin cell with 14 mm of Zn metal foil (250 μm). 2 M $ZnSO_4$ was used as the electrolyte, and each membrane was stored in the 2 M $ZnSO_4$ for more than 24 hours before being applied to Zn symmetric coil cell. The cell was cycled at 1 mA h cm^{-2} at 1 mA cm^{-2}. After 5 cycles, Zn plating was performed for 1 mAh cm^{-2}, and the morphology of Zn deposition was observed depending on membranes through SEM. Additionally, to demonstrate that membranes are capable of uniform Zn deposition, short-circuit time measurements were performed in a Zn symmetric cell. The short-circuit time was determined from the time required for the cell voltage to suddenly fluctuate at 1 mA cm^{-2}.

Optimization of U-A and U-AS amount depending on the membrane properties

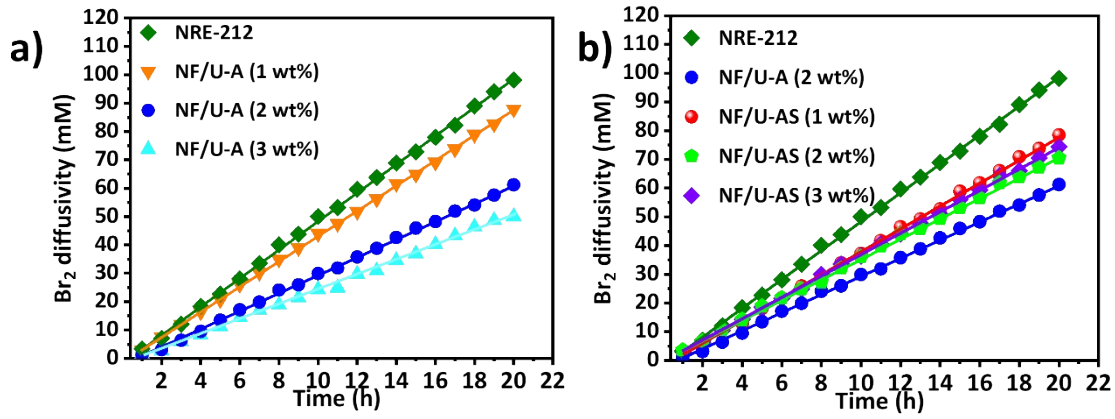

Fig. S24 The Br_2 diffusivity: a) NF/U-A membranes according to different U-A amounts and b) NF/U-AS membranes according to different U-AS amounts. The NRE-212 membrane was used for comparison.

To optimize the U-A and U-AS content in the polymer matrix as a composite membrane, membrane properties were investigated according to U-A and U-AS amount, respectively. The U-A and U-AS contents of 1.0, 2.0, and 3.0 wt% were introduced based on the weight of the Nafion membrane not containing any additive.

First, the Br_2 diffusivity was measured at different times to confirm the Br_2 crossover through the membrane (Fig. S24). In the case of optimization for U-A content, as the U-A content increased, a greater amount of Br_2 was captured, demonstrating lower Br_2 diffusivity (Fig. S21a). As a result, the NF/U-A (3 wt%) exhibited the lowest Br_2 crossover property. The NF/U-AS membranes indicated low Br_2 diffusivity in the order of NF/U-AS 1 wt% < NF/U-AS 2

wt% and NF/U-AS 3 wt% (Fig. S24b). However, no significant differences were found in Br_2 diffusivity of NF/U-AS membranes depending on the U-AS amount introduced. As the U-AS content in the U-AS-based membrane varies, the sulfonic group on the surface of the U-AS also becomes different, not following the same trend as U-A based membranes.

In addition to Br_2 diffusivity, the membrane properties such as area-specific resistance (ASR), ion conductivity, the concentration at which Br_2 crossover occurred based on 12 hours, water uptake and contact angle are summarized in Table S4. The NF/U-A 3 wt% membrane had the lowest ion conductivity as a high amount of the U-A interacted with the sulfonic group of Nafion. Even though the NF/U-AS membranes were introduced into the Nafion matrix, they maintained ion conductivity as the NF/U-AS did not suffer the loss of the ion-conducting group due to the functionalization of the sulfonate group on U-AS. In particular, NF/U-AS (2 wt%) was determined to be the optimal amount based on appropriate ionic conductivity, high hydrophilicity of the surface, large electrolyte absorption ability, and low crossover property. NF/U-A was also determined to be 2 wt%, which has the most suitable properties among NF/U-A membranes with a content of 1 to 3 wt%. Based on the results, NF/U-A (2 wt%) and NF/U-AS (2 wt%) were referred to as NF/U-A and NF/U-AS, respectively, and the battery performances with the comparison of membrane characteristics were dealt with in the main script.

Table S4. Summary of membrane properties for NF/U-A and NF/U-AS membranes depending on the additive amount

Membranes	Water uptake (%)	Contact angle (°)	Ion conductivity (mS cm^{-1})	Br_2 concentration at 12 h (10 mM L^{-1})
NRE-212	24.20	58.55	12.37	59.67
NF/U-A (1 wt%)	23.01	65.27	7.85	51.80
NF/U-A (2 wt%)	21.86	67.67	3.38	35.79
NF/U-A (3 wt%)	22.45	76.07	2.45	29.75
NF/U-AS (1 wt%)	32.14	35.98	12.29	46.63
NF/U-AS (2 wt%)	34.12	31.21	12.21	44.05
NF/U-AS (3 wt%)	35.87	23.40	12.12	44.05

References

1 S. Hee Han, S. Kim, H. Yong Lim, S. Park, K. Shin, S. Kim, H. T. Kim, S. Kyu Kwak, C. Yang and N. S. Choi, *Chem. Eng. J.*, 2023, **464**, 142624.

2 J. H. Lee, Y. Byun, G. H. Jeong, C. Choi, J. Kwen, R. Kim, I. H. Kim, S. O. Kim and H. T. Kim, *Advanced Materials*, 2019, **31**, 1–10.

3 Y. Zhang, C. Wei, M. X. Wu, Y. Wang, H. Jiang, G. Zhou, X. Tang and X. Liu, *Chemical Engineering Journal*, 2023, **451**, 138915.

4 L. Gao, Z. Li, Y. Zou, S. Yin, P. Peng, Y. Shao and X. Liang, *iScience*, 2020, **23**, 101348.

5 S. Liu, J. Wu, J. Huang, X. Chi, J. Yang and Y. Liu, *Sustain Energy Fuels*, 2022, **6**, 1148–1155.

6 W. Wu, S. Xu, Z. Lin, L. Lin, R. He and X. Sun, *Energy Storage Mater*, 2022, **49**, 11–18.

7 P. Xu, C. Xie, C. Wang, Q. Lai, W. Wang, H. Zhang and X. Li, *Chemical Communications*, 2018, **54**, 11626–11629.